Interannual variability of stratospheric and tropospheric ozone determined from satellite measurements

Jack Fishman, John K. Creilson,[1] and Amy E. Wozniak[1]
NASA Langley Research Center, Hampton, Virginia, USA

Paul J. Crutzen[2]
Max-Planck-Institute for Chemistry, Mainz, Germany

Received 10 February 2005; revised 3 May 2005; accepted 3 August 2005; published 28 October 2005.

[1] Long-term satellite records have been used in previous studies to examine both trends and interannual variability (IAV) of ozone in the stratosphere. In this study, we use satellite measurements to produce long-term records of both tropospheric and stratospheric ozone and we examine the IAV of these data sets. Our analysis of the stratospheric component of these observations is consistent with previous findings for total ozone that show a strong correlation with the quasi-biennial oscillation (QBO) at low latitudes. For tropospheric ozone, we find that there are strong regional enhancements due to in situ generation from large emissions. The IAV of some of these regional enhancements, on the other hand, are strongly correlated with the phase of El Niño–Southern Oscillation (ENSO) and are consistent with our understanding of how regions of subsidence are more conducive to the in situ production of ozone pollution. The insight gained from this study will hopefully provide a better understanding between prevailing meteorological conditions and the evolution of widespread ozone episodes on shorter timescales with the eventual goal of producing an air quality forecasting capability so that exposure of the human population to elevated levels of ozone can be reduced.

Citation: Fishman, J., J. K. Creilson, A. E. Wozniak, and P. J. Crutzen (2005), Interannual variability of stratospheric and tropospheric ozone determined from satellite measurements, *J. Geophys. Res.*, *110*, D20306, doi:10.1029/2005JD005868.

1. Introduction

[2] Elevated ozone concentrations produced as a result of fossil and domestic fuel combustion contribute to a number of human ailments such as respiratory diseases [*Spektor et al.*, 1988; *Koren et al.*, 1989; *Lippmann and Schlesinger*, 2000]. Furthermore, the recent study by *Bell et al.* [2004] shows that moderate increases in tropospheric ozone concentrations of only 10 ppbv lead to increased rates of mortality in U.S. metropolitan areas that translate to nearly 4000 premature deaths annually. Other studies have also shown that elevated surface ozone concentrations have deleterious effects on both crop production [*Heck et al.*, 1983] and specific types of plants [*Skelly*, 2000] at concentrations well below the current NAAQS standard of 80 ppbv. On a global scale, surface ozone concentrations have increased significantly during the past century [*Volz and Kley*, 1988; *Staehelin et al.*, 1994] because of increased anthropogenic emissions from industrial and agricultural processes. The concurrent increased emissions of nitrogen oxides and hydrocarbons in the presence of sunlight are the primary factors leading to these higher concentrations of ozone.

[3] The long-term data record of tropospheric ozone residual (TOR) distributions (http://asd-www.larc.nasa.gov/TOR/data.html) has used concurrent measurements from the Total Ozone Mapping Spectrometer (TOMS) and Solar Backscattered Ultraviolet (SBUV) instruments to develop a quasi-global tropospheric ozone climatology [*Fishman et al.*, 2003]. This climatology shows significant regional enhancements of ozone pollution resulting from the release of copious emissions from regionally industrialized areas in the Northern Hemisphere and widespread biomass burning in the tropics. In addition to the climatological and seasonal distributions discussed by *Fishman et al.* [2003], this data record spans more than two decades (1979–2000) yielding nearly 17 years of monthly averaged depictions. Within this record, there is significant interannual variabiltiy (IAV) of elevated pollution in certain regions. Because of the unique length and data density of this tropospheric trace gas database, it is possible, for the first time, to examine the IAV of the TOR and to see if this IAV can be correlated with other well-known IAV parameters: The quasi-biennial oscillation (QBO) and the El Niño–Southern Oscillation (ENSO).

[4] Another objective of this study is to examine a complimentary integrated data set that is also derived from

[1] Also at Science Applications International Corporation (SAIC), Hampton, Virginia, USA.
[2] Also at Scripps Institute of Oceanography, La Jolla, California, USA.

0148-0227/05/2005JD005868$09.00

Region	Lat	Monthly SCO Correlations											
		Jan	Feb	Mar	Apr	May	Jun	Jul	Aug	Sep	Oct	Nov	Dec
	N=>	18	18	17	18	17	17	17	18	18	18	17	17
West Africa (20W-30E)	15-20N	-.23	-.34	-.37	**-.48**	-.39	-.12	.07	-.20	-.20	-.20	-.10	-.17
	10-15N	.18	.03	-.06	-.09	.12	.27	.44	.09	.10	.05	.16	.13
	5-10N	**.55**	.46	.40	.31	**.53**	**.57**	**.71**	**.53**	**.56**	**.54**	**.55**	**.52**
	E-5N	**.64**	**.63**	**.67**	**.60**	**.71**	**.73**	**.82**	**.73**	**.74**	**.72**	**.70**	**.65**
	E-5S	**.53**	**.65**	**.68**	**.66**	**.74**	**.73**	**.83**	**.70**	**.64**	**.63**	**.70**	**.54**
	5-10S	.36	**.56**	**.56**	**.57**	**.62**	**.49**	**.59**	.34	.26	.33	**.56**	.27
	10-15S	.11	.37	.31	.25	.18	.02	-.15	**-.49**	-.35	-.37	-.10	-.14
	15-20S	-.10	.13	.01	-.16	-.31	-.31	**-.55**	**-.78**	**-.68**	**-.65**	**-.51**	-.38
India (60-120E)	15-20N	-.28	-.17	-.40	-.45	-.48	-.27	.11	-.04	.04	.15	-.08	-.31
	10-15N	.21	.23	-.02	-.17	.05	.18	.38	.21	.36	.40	.23	-.08
	5-10N	**.60**	**.64**	**.49**	.41	**.52**	**.52**	**.64**	**.53**	**.67**	**.70**	**.73**	.44
	E-5N	**.65**	**.69**	**.67**	**.69**	**.67**	**.63**	**.78**	**.72**	**.80**	**.79**	**.87**	**.65**
	E-5S	**.62**	**.66**	**.68**	**.73**	**.71**	**.65**	**.78**	**.73**	**.79**	**.74**	**.83**	**.58**
	5-10S	**.54**	**.59**	**.57**	**.66**	**.62**	.35	**.50**	.35	**.47**	**.48**	**.67**	.34
	10-15S	.30	.41	.27	.34	.22	-.21	-.33	**-.48**	-.42	-.26	-.04	-.27
	15-20S	.02	.20	-.06	-.13	-.23	-.45	**-.64**	**-.69**	**-.68**	**-.56**	**-.57**	**-.49**
Pacific (160-100W)	15-20N	-.34	-.19	-.37	-.36	**-.53**	-.17	.02	-.09	-.17	-.03	-.06	-.18
	10-15N	-.02	.08	-.03	-.11	-.13	.17	.32	.17	.12	.23	.27	.11
	5-10N	.34	.44	.40	.28	.30	**.49**	**.65**	**.51**	**.47**	**.55**	**.69**	**.54**
	E-5N	**.53**	**.63**	**.65**	**.57**	**.56**	**.69**	**.79**	**.67**	**.59**	**.65**	**.79**	**.65**
	E-5S	**.50**	**.64**	**.73**	**.67**	**.63**	**.72**	**.78**	**.66**	**.54**	**.58**	**.71**	**.59**
	5-10S	.29	**.49**	**.63**	**.56**	**.53**	**.55**	.45	.35	.21	.26	.42	.34
	10-15S	.02	.25	.38	.19	.19	.10	-.35	**-.49**	**-.51**	-.43	-.29	-.09
	15-20S	-.14	.08	.15	-.22	-.25	-.32	**-.71**	**-.80**	**-.80**	**-.69**	**-.63**	-.33

Key (all correlations in **bold** are significant to at least the .05 level):

Positive Correlation and level of significance of at least .01:
Positive Correlation and level of significance of at least .05:
Negative Correlation and level of significance of at least .01:
Negative Correlation and level of significance of at least .05:

Figure 1. Correlation coefficients between stratospheric column ozone (SCO) and one of the quasi-biennial oscillation (QBO) indices (wind speed at 30 hPa over Singapore), displayed as a function of month and latitude. Instead of using zonally averaged SCO quantities, these correlations have been computed for three different east-west domains: near the Prime Meridian over and south of west Africa, south of India, and over the eastern Pacific. The blue and green regions indicate strong positive correlations (generally near the equator and at all times of the year) whereas the yellow and orange regions indicate regions of anti-correlation (generally at southern subtropical latitudes during austral spring).

the TOR methodology applied to the TOMS and SBUV measurements. The stratospheric column ozone (SCO) is the integrated amount of ozone above the tropopause and its climatological distribution is in excellent agreement with a comparable quantity derived from Stratospheric Aerosol and Gas Experiment (SAGE) profiles [*Wozniak et al.*, 2005]. Thus, in this study, we also show that the IAV of SCO is consistent with earlier studies that have examined the relationship between TOMS total ozone and the QBO, leading to an important confirmation of the use of TOR methodology to investigate IAV behavior.

[5] On the other hand, the regional and long-term nature of the TOR fields is a unique attribute of this data set. Whereas the QBO is observed on a significantly large spatial scale in the stratosphere, we find that some of the regions where significant air pollution is found display IAV that is highly correlated with ENSO. Such a relationship may provide important insight for determining when prolonged elevated pollution events may be conducive to formation, and possibly even lead to identifying specific meteorological situations that portend pollution episodes.

2. Derivation of Data Set Used in this Study

[6] TOMS total ozone measurements have been available from several satellites since November 1978 (see http://toms.gsfc.nasa.gov). Nimbus-7 operated from November 1978 through April 1993; the Earth Probe satellite operated at a relatively low orbit of 540 km and provided higher spatial resolution from July 1996 through December 1997 and then was boosted to a higher orbit of 740 km to obtain complete global coverage. For the current study, Nimbus-7

TOMS data (Version 7) from 1979 through 1993 and Earth Probe data from 1997 through 2000 have been analyzed. Only data from the Nimbus-7 and Earth Probe have been used in this study to take advantage of the availability of the aerosol index information that is part of the correction we apply to the measurements [*Torres and Bhartia*, 1999; *Fishman and Balok*, 1999].

[7] The SCO is determined from SBUV profiles integrated from the tropopause to the top of the atmosphere. Before integration above the tropopause, each SBUV profile is empirically corrected so that the amount of ozone below the tropopause is set equal to the monthly climatological amount determined from the *Logan* [1999] analysis. This quantity is then subtracted from the SBUV total ozone column to derive the SCO [*Fishman and Balok*, 1999; *Fishman et al.*, 2003]. That value (i.e., the integrated ozone amount above the tropopause derived from the SBUV measurement) is then used as input to derive a stratospheric ozone field using other such measurements over a 5-day period to determine the field for the central day. That quantity is then subtracted from the concurrent TOMS total ozone amount on the central day to calculate the TOR for this study. Tropopause height information for the current study uses gridded (2.5° latitude by 2.5° longitude) analyses provided by the National Centers for Environmental Prediction (NCEP). These analyses are produced every 6 hours and the value closest to the time of the SBUV observation is used in the current study. For the discussion presented in the following sections, we present monthly maps that have been derived from the TOR distribution calculated daily and then averaged over the month.

3. Stratospheric and Tropospheric IAV in the Tropics

3.1. Relationship Between Stratospheric Ozone and the QBO

[8] In addition to quantifying the global nature of secular trends in stratospheric ozone depletion, long-term total ozone satellite measurements (i.e., TOMS and SAGE) have been used to investigate multiyear cycles that also can be found in these data records [*Bowman*, 1989; *Chandra and Stolarski*, 1991; *Tung and Yang*, 1994; *Kinnersley and Tung*, 1998]. One of the strongest and most clear-cut signals found in these total ozone records is that of the quasi-biennial oscillation (QBO), a feature that was first observed for stratospheric equatorial winds [*Reed*, 1965]. The QBO is a well-documented meteorological phenomenon [*Lindzen and Holton*, 1968] in which the zonal winds in the lower stratosphere change direction with a periodicity of 24–30 months. In accordance with this change of wind direction, the amount of ozone in the stratosphere also changes where a strong westerly component is associated with relatively higher amounts of ozone while an easterly component is associated with relatively lower amounts. In addition, the analysis of SAGE O_3 profile data has shown that the QBO signal propagates throughout vertically within the stratosphere [*Hasebe*, 1996; *Randel and Wu*, 1996].

[9] In this section, we examine the relationship between the stratospheric column ozone (SCO) and parameters that can be used to define QBO. *Kinnersley and Tung* [1998] have provided a comprehensive analysis of the correlation between TOMS total ozone and stratospheric winds over Singapore. In Figure 1, we present a similar analysis, but instead of using complete zonal averages, we break the equatorial regimes into three regions: West Africa (20°W–30°E); India (60°E–120°E); and Central Pacific (160°W–100°W) (QBO data courtesy of University of Washington and can be found at http://tao.atmos.washington.edu/data_sets/qbo/). Furthermore, instead of using TOMS total ozone, we use the monthly SCO values that are derived through our calculation of TOR using coincident TOMS total ozone information and profile information from SBUV measurement between 1979 and 2000. The number of monthly SCO values going into the correlation coefficient calculations is shown as the first number in each column. Our findings of the relationship between the SCO and the QBO at low latitudes are qualitatively the same as those of *Kinnersley and Tung* [1998] using a 13-year record of TOMS and Singapore winds from 1980–1993. In the band along the equator (5°N–5°S), 63 of the 72 correlation coefficients show a level of significance of at least 0.01, meaning that there is less than a 1% chance that the two sets of data are not correlated; the remainder of the correlation coefficients in these latitude bands have a level of significance of 0.05, implying that there is less than a 5% chance that the QBO and SCO values are not correlated. The monthly correlations become less positive when they are calculated farther away from the equator. Furthermore, there is an anti-correlation in the southern subtropics (15°S–20°S) during late austral winter through austral spring (July–November). Kinnersley and Tung's correlation analysis yielded nearly identical findings where the austral spring anti-correlation extended to southern middle and high latitudes (regions not of interest in this study). In the discussion that follows, it is significant that the IAV for the SCO data behave in a manner that is consistent with our understanding of stratospheric dynamics and that the nature of this behavior at low latitudes is regionally independent (as defined

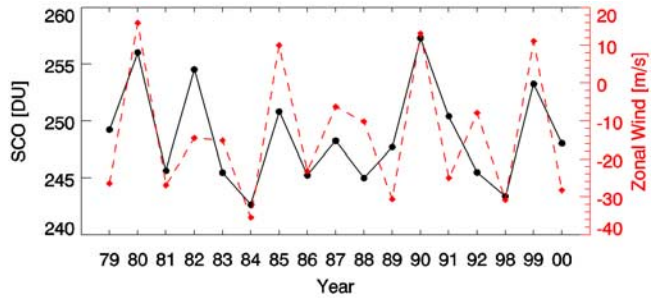

Figure 2. Solid black line showing a time series of the monthly average amount of ozone in the stratosphere (stratospheric column ozone, SCO), for July for years for which there are data between 1979 and 2000 for the equatorial region (5°N–10°N) between 20°W and 30°E (West Africa); dashed red line shows the mean zonal for July at 30 hPa over Singapore (one index used to define the phase of the QBO). The correlation coefficient for these two variables is +0.72.

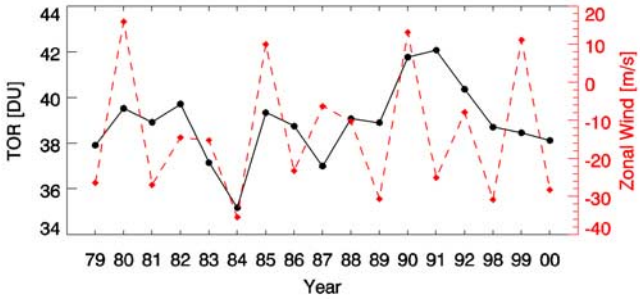

Figure 3. Average amount of tropospheric ozone for each July over the West Africa region plotted against the same QBO index as shown in Figure 2. The correlation coefficient between these two variables is 0.36, which is not significant.

by the three regions in Figure 1). A specific time series for the month of July is shown in Figure 2 where the SCO for the West Africa box defined in Figure 1 is plotted as a function of year against the monthly average zonal wind measured over Singapore at 30 hPa, a commonly used indicator of the phase of the QBO. The correlation coefficient of the two variables in this time series is +0.72.

3.2. Interannual Variability Over West Africa

[10] Although the IAV of equatorial stratospheric ozone is dominated by dynamical processes related to the QBO, the ozone distribution in the troposphere is correlated to a significantly less degree with the QBO. The plot shown in Figure 3 is similar to the one shown in Figure 2 except it shows the relationship between the July TOR over the same region over West Africa and the QBO. These two variables have a correlation coefficient of 0.36, which is not significant with this number of data points.

[11] ENSO indices, which consist of the Southern Oscillation Index (SOI) and equatorial Pacific Ocean sea surface temperature anomalies (SSTAs), are illustrated in Figure 4 (image provided by NOAA Climate Prediction Center from their web site at http://www.cpc.ncep.noaa.gov). The original SOI was defined as the pressure difference between Darwin (northern Australia) and Tahiti (central equatorial Pacific) [*Philander*, 1990]. More recent definitions of ENSO use sea surface temperature variations in regions of the equatorial Pacific to define the strength of the phase of El Niño; specifically, these indices quantify the departure from the average temperature (sea surface temperature anomaly, SSTA) in specific regions. Region 1 + 2 is a relatively small area in the extreme eastern Pacific near the Peruvian coast, the region first recognized as changing significantly during the ENSO cycle. In more recent times, when technology developed so that more remote regions could be monitored, other larger areas of the Pacific were defined and found to be generally more impacted by the coupled ocean-atmosphere nature of the ENSO. Thus Region 3 is a larger area encompassing the equatorial eastern Pacific whereas Region 4 has been defined as the box in the western/central Pacific; by convention, Region 3.4 denotes the central Pacific. For the discussion on the TOR over West Africa that follows, we will use the standard SOI index to examine the relationship between ENSO and tropospheric ozone. We will also refer to the various SSTAs in later discussions. The SCO and SOI correlation coefficient for June in this region is a statistically insignificant 0.26.

[12] An example of the IAV in the TOR field is clearly illustrated by the distributions shown in Figure 5 where significantly more ozone is observed during June over western Africa during 1982, a strong El Niño year, as compared to 1984, a strong La Niña year. In addition to a weaker relationship (but still sometimes significant) between TOR amounts and the QBO over western Africa, we have found that the pattern of the distribution is at times highly correlated to the phase of ENSO. To define this pattern, we examine the difference in the amount of ozone north and south of the equator: $\Delta(\mathrm{TOR}) = \mathrm{TOR}_{5°\mathrm{N}-10°\mathrm{N}} - \mathrm{TOR}_{5°\mathrm{S}-10°\mathrm{S}}$. Figure 6 illustrates the strong nature of this correlation for the month of June, where Δ(TOR) is compared with the Sea Surface Temperature Anomaly (SSTA)

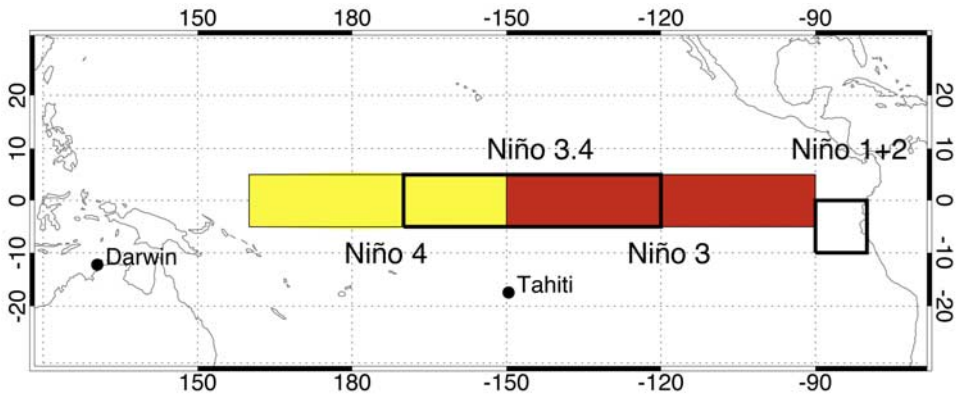

Figure 4. Graphical depiction of the Sea Surface Temperature Anomaly Regions used to define ENSO intensity: Niño region 1 + 2 is the area off the coast of Ecuador; Region 3 is the red box in the eastern Pacific; Region 4 is the yellow box in the western Pacific; Region 3.4 is the overlapping area in the central Pacific. The classic Southern Oscillation Index (SOI) is defined as the difference between the surface pressure at Darwin, Australia, and Tahiti.

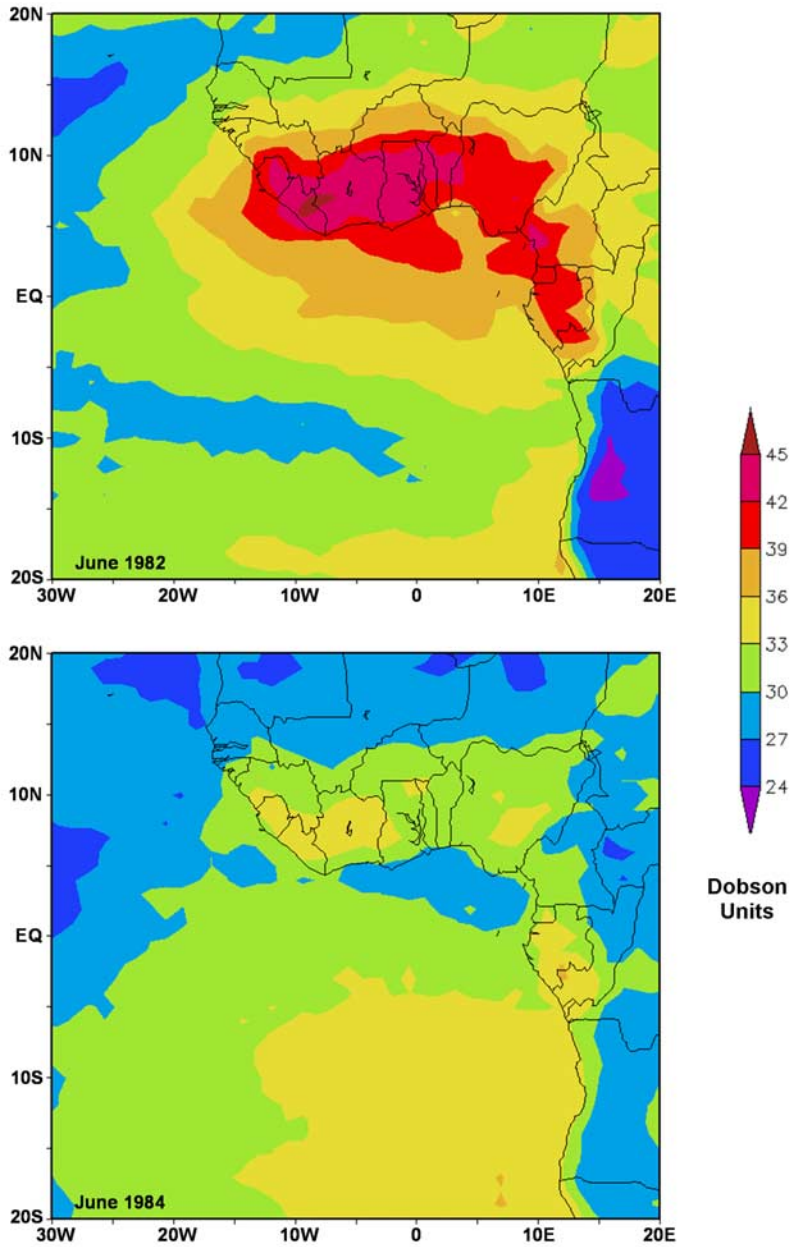

Figure 5. Depiction of the interannual variability of tropospheric ozone during June of a strong El Niño year (1982) and June of a strong La Niña year (1984).

observed over the west central Pacific (El Niño Region 4), where the resultant correlation coefficient for these two variables is 0.78.

[13] *Cook* [1999] investigated the meteorology over this region through an analysis of the African Easterly Jet (AEJ) and precipitation over West Africa. He found that during the summer months the climatological African Easterly Jet formed in the presence of a negative soil moisture gradient, peaking at approximately 15°N. The jet, which is typically located at ~600 hPa, is driven by the difference in strong summer insolation and dryness over Saharan Africa to the north and the wet season over West Africa and western Sahelian Africa to the south. Several studies show that anomalously drier summers are linked to a southward displacement of both the Intertropical Convergence Zone (ITCZ) and the AEJ [*Grist and Nicholson*, 2001; *Nicholson and Grist*, 2003]. This southward displacement means that the precipitation processes (i.e., the West African summer monsoon) that the AEJ/ITCZ help drive also setup farther south, creating a situation where subsidence is prevalent over this region of West Africa.

[14] Earlier studies linked the phase of ENSO with African rainfall, through an analysis of the phase of a defined 2-year ENSO cycle and its relationship with the strength of the Atlantic and Indian Ocean SSTAs [e.g., *Nicholson and Kim*, 1997]. Similarly, we find that during the summers of El Niño years (as defined by the June El Niño 4 SSTAs), the AEJ and ITCZ appear to be displaced

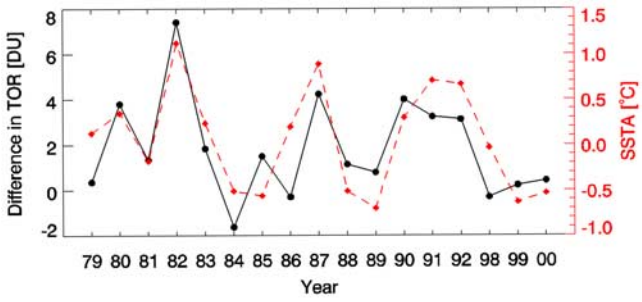

Figure 6. A measure of the North/South gradient ($TOR_{5°N-10°N} - TOR_{5°S-10°S}$) plotted as the black solid line; the Sea Surface Temperature Anomaly in the west/central Pacific Ocean, a measure of the phase of the ENSO, is shown by the dashed red line. The correlation coefficient between these two variables is 0.78.

farther south, and that vertical velocity (ω) over our West African study region is anomalously positive. Figure 7 (image provided by the NOAA-CIRES Climate Diagnostics Center, Boulder Colorado from their Web site at http://www.cdc.noaa.gov/[*Kalnay et al.*, 1996]) shows the average vertical velocity at 700 hPa over this region during the "El Niño" years (Figure 7, top) and the distribution of the correlation coefficient between ω and the SOI index over the period 1979–2000 (Figure 7, bottom). These depictions suggest that meteorological conditions during El Niño years favor strong subsidence in the lower troposphere over this region. In addition to the increased subsidence, the meteorological data [*Kalnay et al.*, 1996] also clearly show that both the precipitation amounts and rate are considerably lower during the El Niño summers relative to other years.

[15] The presence of widespread subsidence can be conducive to enhanced ozone in the troposphere for several reasons. When rain is reduced, the relatively drier land and clearer skies provide more favorable conditions for widespread vegetation burning which can lead to larger amounts of ozone precursors being emitted. Such conditions are also conducive to more sunshine and thus ozone being generated more efficiently through enhanced photochemical activity. Last, widespread subsidence would more efficiently bring higher levels of ozone down from the upper troposphere and lower stratosphere. Unfortunately, the sources of elevated TOR values cannot be differentiated without in situ measurements that better define the vertical structure of ozone within the troposphere.

4. IAV of Tropospheric Ozone Over Northern India and East China

[16] The use of satellites to measure the distribution of tropospheric trace gases has provided a new appreciation for how local and regional emissions strongly influence the resultant global distribution of these trace species. Figure 8 (top) [*Boersma et al.*, 2004] shows that NO_2 emissions come predominately from northern temperate latitudes and to a lesser extent from tropical Africa and South America. The satellite-derived TOR product shows considerably greater amounts in NH summer (Figure 8, bottom) when sunlight is sufficiently prevalent to generate ozone efficiently. Recent depictions for satellite-derived carbon monoxide distributions also show emissions emanating from regions of high anthropogenic activity and widespread tropical biomass burning [*Edwards et al.*, 2003; *Frankenberg et al.*, 2005].

[17] There have also been recent studies showing a relationship between satellite-derived tropospheric column ozone (TCO) amounts and the phase of the ENSO cycle in the tropics [*Ziemke and Chandra*, 2003]. In that study, they compared TCO data at two tropical locations, Tahiti and Darwin, with the difference in pressure at those two sites (the conventional definition of the Southern Oscillaiton Index, SOI) and found a significant statistical relationship in the TCO gradient between the two sites and the SOI. In

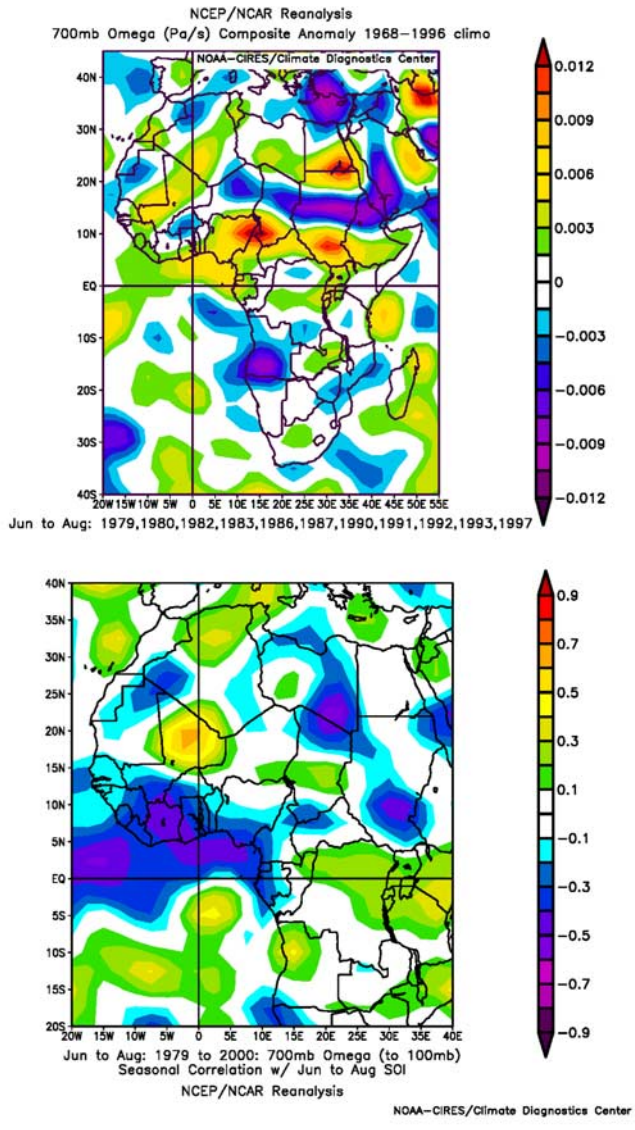

Figure 7. (top) An analysis of June–August vertical velocity, ω (omega), at 700 hPa over West Africa during El Niño years (1979, 1980, 1982, 1983, 1986, 1987, 1990, 1991, 1992, 1993, 1997). Positive ω_{700} is indicative of subsidence. (bottom) Distribution of the correlation coefficient between ω and the SOI index over Africa. Strongest correlation is found over Gulf of Guinea region.

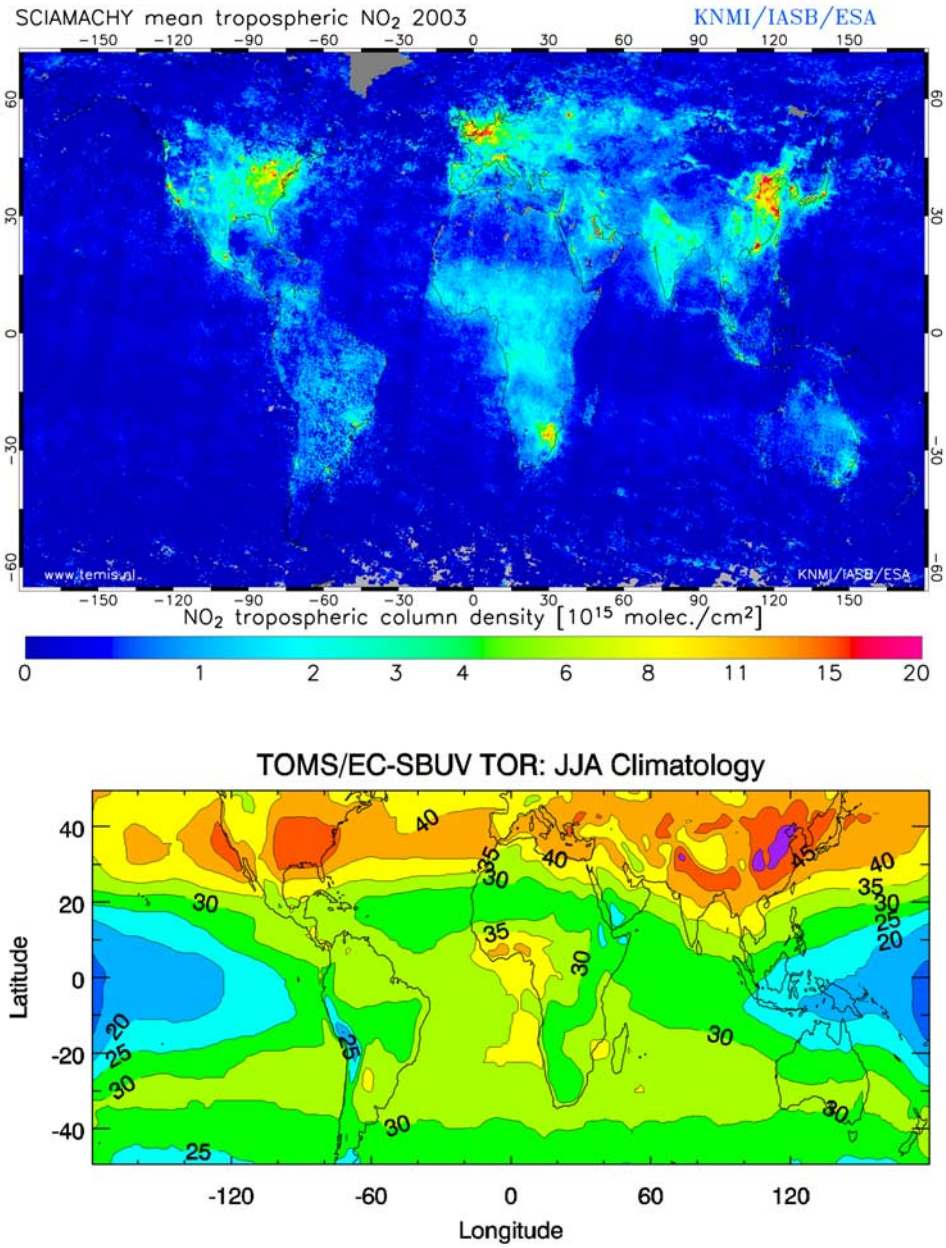

Figure 8. (top) Distribution of tropospheric NO_2 derived SCIAMACHY for the year 2003 [*Boersma et al.*, 2004]. (bottom) Climatological TOR distribution during June-July-August [*Fishman et al.*, 2003].

this study, we expand on the finding first noted by *Ziemke and Chandra* [2003] by examining a region that is prone to pollution [*Di Girolamo et al.*, 2004] to determine whether or not the intensity of the pollution can be linked to the ENSO cycle.

[18] Of particular interest is the region in northern India where *Di Girolamo et al.* [2004] also observe a "pollution pool" based on aerosol optical depth measurements from 4 years of Multiangle Imaging SpectroRadiometer (MISR) measurements. The amount of tropospheric ozone over this region as well as in eastern China follows a well-defined seasonal cycle (see Table 1) with a peak in the summer, when photochemical ozone generation is highest. In addition to this seasonal cycle, however, the Indian data suggest the interannual variability within our 1979–2000 data set is strongly correlated with the ENSO indices previously discussed (see Figure 4). The correlation between the interannual variability of the TOR with these indices suggests a strong relationship between the ENSO and the amount of ozone pollution in northern India during the summer (Table 2). Conversely, Table 2 shows that no such relationship is observed over China.

[19] The significant associations shown in Table 2 also correspond with the timing of the monsoon season in this

Table 1. Summary of TOR Values Over Northern India Study Region[a]

Month	Mean TOR (DU)	Range (DU) High	Range (DU) Low
	Northern India		
January	29.9	31.6 (1998)	25.4 (1980)
February	29.7	33.7 (1992)	24.8 (1991)
March	34.7	40.4 (1989)	27.1 (1999)
April	44.1	47.3 (1982)	40.4 (1985)
May	47.4	53.0 (1982)	42.4 (1998)
June	48.1	52.4 (1982)	44.8 (1999)
July	46.5	48.5 (1982)	43.6 (1999)
August	42.3	44.1 (1992)	40.0 (1999)
September	36.9	40.3 (1990)	35.0 (1979)
October	32.8	34.7 (1999)	30.5 (1987)
November	30.5	33.3 (1981)	28.6 (1984)
December	27.9	29.9 (1985)	25.6 (1984)
	China		
January	27.4	30.3 (1988)	24.1 (1991)
February	30.4	33.9 (1990)	27.5 (1992)
March	34.9	39.5 (1992)	31.5 (1998)
April	41.3	45.1 (1984)	38.4 (1990)
May	45.9	49.6 (1992)	41.3 (1988)
June	50.7	55.4 (1979)	48.5 (1991)
July	50.7	53.8 (1990)	49.0 (1982)
August	46.8	48.6 (1999)	44.8 (1979)
September	40.0	41.8 (1998)	38.1 (1979)
October	34.5	38.6 (1998)	32.0 (1992)
November	31.4	33.6 (1979)	28.7 (1989)
December	27.9	30.6 (1982)	25.6 (1984)

[a]All values are in Dobson Units (DU). The first column shows the average TOR by month over this region. The second and third columns show the high and low years, respectively (and the year in which these extremes occurred).

region. The monsoon season, like the TOR, exhibits considerable interannual variability [*Krishnamurthy and Shukla*, 2000; *Goswami and Mohan*, 2001]. Figure 9 shows a time series of the summer TOR over northern India and the SSTA in Region 4. During summers of increased TOR (1982, 1987, 1991–1992), it should be noted that there is also reduced rainfall [*Parthasarathy et al.*, 1995]. Coincidently, these same years correspond to the warm phase of ENSO (i.e., ''El Niño'' years). A major factor contributing to monsoonal variability has been its relationship with the ENSO phenomenon. Drought years over India during the summer monsoon are often, but not exclusively, associated with warmer SSTAs in the equatorial central and eastern Pacific (El Niño) and wet years with relatively colder SSTAs (La Niña) [*Rasmusson and Carpenter*, 1983; *Webster and Yang*, 1992; *Ju and Slingo*, 1995]. One factor driving the monsoon-ENSO connection is the modulation in the latitudinal shift of the ITCZ exhibited during a warm phase of the preceding spring, which may be delaying the onset of the monsoon [*Ju and Slingo*, 1995]. The delayed northward shift in the ITCZ can affect the development of the Somali Jet and subsequent onset of the southwest monsoonal flow. This delayed onset has been shown to lead to a weakened large-scale monsoonal circulation (Somali jet) and thus a weaker monsoon overall (i.e., less precipitation) [*Shukla and Wallace*, 1983; *Ju and Slingo*, 1995]. During this phase, the Walker Circulation can actually weaken or reverse itself, causing subsequent changes in surrounding circulation regimes. Associated with this ITCZ shift and change in the Walker Circulation is increased convection over the east Pacific and increased subsidence over the western Pacific and east Asia. This increased subsidence has also been linked to a weaker monsoon season [*Shukla and Wallace*, 1983; *Palmer et al.*, 1992]. Thus the relationship of increased tropospheric ozone to the warm phase of ENSO could be due to the increased subsidence over southeast Asia (analogous to what is observed over west Africa) and a weakened Somali jet, leading to a drier monsoon season. A drier monsoon season could lead to either increased burning or enhanced photochemical activity due to less cloudiness since either factor would lead to enhanced in situ production of tropospheric ozone [e.g., *Fishman et al.*, 1987].

[20] Examination of the relationship between the ENSO cycle and the amount of ozone over China (Table 2) shows that there are no statistically significant correlations between the TOR and any monthly or seasonal SOI or SSTA regions. Some of the correlations are as high as 0.40 (values with 95% confidence levels should be $\sim|0.48|$ or greater), but the sign of these correlations is opposite of what is seen in the India data.

[21] There is the possibility that increased cloud cover over this region during the summer monsoon period impacts

Table 2. Monthly and Seasonal Correlation Coefficients Between the TOR Over This Region and the SOI Index and Sea Surface Temperature Anomalies (SSTAs) in the ENSO SST Regions Shown in Figure 4[a]

Month	SOI Monthly	SOI Seasonal	ENSO SST Region 1 and 2	3	3.4	4
			India-ENSO Correlations			
January	−0.06	−0.09	0.15	0.06	0.03	0.05
February	−0.34	−0.48	0.12	0.28	0.34	0.23
March	0.03	0.02	−0.14	−0.13	−0.06	0.11
April	−0.15	−0.14	−0.14	0.05	0.12	0.24
May	0.22	0.24	−0.20	0.08	0.13	0.30
June	−0.43	**−0.55**[b]	−0.11	0.27	0.41	0.44
July	−0.48	**−0.56**[b]	0.06	0.40	**0.59**[b]	**0.68**[c]
August	−0.44	**−0.53**[b]	0.12	0.45	**0.57**[b]	**0.66**[c]
September	0.13	0.19	−0.25	−0.25	−0.23	0.04
October	**0.50**[b]	0.43	−0.36	−0.43	−0.47	**−0.54**[b]
November	0.28	0.10	0.12	0.04	−0.01	−0.13
December	**0.50**[b]	0.30	−0.02	−0.09	−0.16	−0.16
			China-ENSO Correlations			
January	−0.22	−0.14	0.12	0.15	0.17	0.19
February	−0.19	−0.09	0.27	0.21	0.19	0.29
March	−0.10	−0.01	−0.21	−0.03	0.15	0.26
April	−0.40	−0.38	−0.05	0.13	0.26	0.27
May	−0.09	−0.07	0.06	0.39	0.39	0.18
June	0.40	0.39	0.17	0.04	0.02	0.04
July	0.31	0.34	−0.38	−0.17	−0.08	−0.07
August	0.06	−0.16	−0.14	−0.07	−0.11	−0.19
September	0.20	0.21	−0.09	−0.28	−0.34	−0.35
October	0.31	0.29	0.16	−0.04	−0.15	−0.40
November	−0.04	−0.19	0.35	0.24	0.18	0.08
December	−0.05	−0.09	0.28	0.35	0.30	0.19

[a]The SOI column refers to the correlation coefficient for each monthly TOR over the period 1979–1999 with the Southern Oscillation Index computed both monthly and seasonally. The last four columns show the correlation coefficient of the monthly TOR with the Sea Surface Temperature Anomalies (SSTA) calculated for the four equatorial Pacific regions shown in Figure 4. Significant correlations are in bold.
[b]Correlations exhibiting a.05 significance level.
[c]Correlations exhibiting a 0.01 significance level.

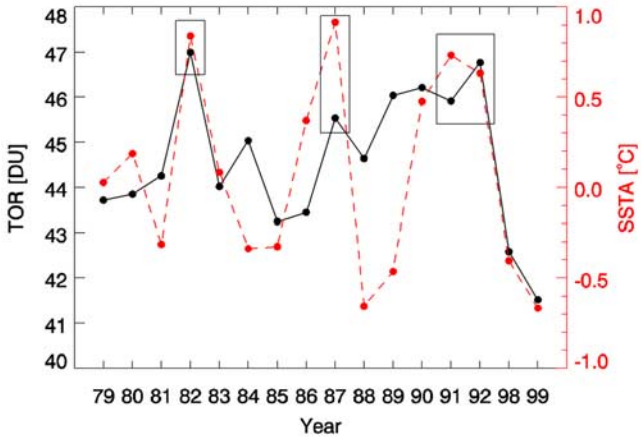

Figure 9. Relationship between summer TOR over India and ENSO Region 4 SSTAs. TOR values over northern India between 1979 and 1999 for the years that complete summertime data are available and the SSTA over the western Pacific (i.e., Region 4, see Figure 4). Blocked areas refer to strong El Niño episodes.

satellite retrievals of ozone. Generation of TOR products used in this study was derived from the TOMS archive (http://toms.gsfc.nasa.gov/ozone/ozone.html) which include cloudy, partially cloudy, and cloud-free pixels. When compared with TOR generated from another version of TOMS data, which allowed us to segregate individual pixels from clear and cloudy areas, the presence of clouds did not produce significant differences in the distributions derived over India and east Asia. Furthermore, validation of gradients of the type shown in this study are supported by the analysis described by *Creilson et al.* [2003], that compared spatial differences in TOR with integrated ozone derived from ozonesonde measurements.

[22] Findings from the Indian Ocean Experiment (INDOEX) confirm the hypothesis that anthropogenic emissions are responsible for the widespread presence of haze and pollution covering much of Asia and the adjacent Indian Ocean [*Lelieveld et al.*, 2001] and that such perturbations may impact the global climate system [*Ramanathan et al.*, 2001]. During the intensive field phase of INDOEX, a number of aircraft measurements found aged pollution plumes during several flights north of the Intertropical Convergence Zone (ITCZ) whose source regions were identified as northeastern India and Bangladesh [*de Gouw et al.*, 2001]. These findings are consistent with the NO_2 distribution shown in Figure 8 and with emissions data [*van Aardenne et al.*, 1999] suggesting that substantial amounts of nitrogen oxides (NO_x) should be present along the Ganges River Valley of northern India and northern Bangladesh. Because NO_x is the most important precursor for the photochemical generation of tropospheric ozone, concurrent presence of high concentrations of O_3 would not be unexpected.

5. Discussion

[23] This study has shown that IAV of ozone in both the troposphere and the stratosphere can be linked to large scale meteorological forcing parameters associated with well-known documented phenomena: the QBO in the equatorial stratosphere and the ENSO in the tropical and subtropical troposphere. We have used monthly averaged information over a 21-year period to relate ozone to these large-scale features that have been shown to exhibit teleconnections over large parts of the globe.

[24] *Duncan et al.* [2003] have used satellite data to show that fire frequency in several regions of the world is directly tied to ENSO-induced droughts. Using Along Track Scanning Radiometer (ATSR) and TOMS Aerosol Index (AI) data, they show large enhancements in Malaysia and Indonesia in biomass burning fires and attendant widespread particulate enhancement during the El Niño periods of 1982–1983, 1991, and 1997–1998. Thus the link between ENSO and increased emissions that should lead to elevated ozone pollution concentrations has been established. Furthermore, *Di Girolamo et al*. [2004] confirm the massive amount of particulate matter present in the same region we find high TOR values in northern India. Thus, on a seasonal basis, it is fairly straightforward to link favored meteorological situations to the formation of widespread pollution.

[25] In an earlier study, *Fishman and Balok* [1999] were able to use TOR data to help interpret the development of a large air pollution episode over the eastern United States in July 1988, which was driven by the development of an unusually intense and expansive high-pressure regime over this region. Clearly, there are prevailing meteorological conditions that optimize the formation of ozone pollution on seasonal as well as on synoptic (3–7 days) timescales. In addition, *Creilson et al.* [2003] have used the IAV of this TOR data set to show a relationship between transcontinental transport and the North Atlantic Oscillation (NAO). The ultimate goal of these kinds of studies is to establish a means of linking specific meteorological situations to the potential onset of elevated ozone periods. This study suggests that such relationships can be done in some regions (west Africa and northern India) in a statistical seasonal sense. Fishman and Balok showed that certain meteorological conditions are conducive to ozone formation on shorter timescales that are even more intense and it is these specific intense episodes that lead to the most pronounced damage to plants, crops, and human health [*Chameides et al.*, 1999; *Cheung and Wang*, 2001]. If we can understand such relationships, and then forecast them correctly in pure meteorological terms, then perhaps we can mitigate the impact of the formation of ozone by reducing regional emissions. As shown by *Bell et al.* [2004], the reduction of surface ozone concentrations by only as little as 10 ppbv could result in lowering premature deaths by several thousand per year in the United States. Extrapolation of such reductions of exposure to high concentrations worldwide would have an enormous benefit that would be difficult to quantify.

6. Summary and Conclusions

[26] We have presented an analysis of interannual variability using a data set that spans more than two decades. This analysis shows that the methodology used to separate the troposphere from the stratosphere in these concurrent measurements from TOMS and SBUV instruments produces

two long-term records that are independent of each other. Our analysis of the IAV of the SCO data reproduces previous findings using TOMS total ozone and SAGE stratospheric ozone profile measurements that show that the amount of stratospheric ozone at low latitudes is highly linked to meteorological processes that drive the QBO. On the other hand, there is a much weaker relationship between the TOR product derived from these same satellite measurements and the QBO. At the same time, we have shown that there is a strong correlation between TOR and ENSO during specific times of the year, but only at specific much smaller scale regimes. The months that favor enhanced levels of tropospheric ozone are consistent with our understanding from a meteorological point of view as to why higher ozone values should be produced; i.e., at times when subsidence is more prevalent and when local precipitation is suppressed.

[27] In recent years, the development of air quality models for understanding the formation of ozone episodes has accelerated with the intent of becoming operational in less than a decade [*Dabberdt et al.*, 2004]. This study, on the other hand, has used historical measurements in an attempt to identify what meteorological regimes have been most conducive to widespread ozone formation on a monthly basis. Relating these monthly distributions to prevailing meteorological conditions will hopefully provide insight into analogous ozone-producing events on smaller timescales that lead to prolonged elevated ozone events providing the eventual capability of relating these situations to what is observed at the surface, as was done by *Fishman and Balok* [1999]. The first use of satellite information being used in near-real-time to improve air-quality forecasts has recently been demonstrated [*Szykman et al.*, 2004; *Al-Saadi et al.*, 2005] with the goal to use such forecasts to warn the public so that they can take measures to reduce exposure to high pollutant concentrations as well as to reduce emissions in specific regions so that less ozone is actually produced. Achieving an understanding between meteorology, satellite measurements representative of tropospheric pollution, and high concentrations at the ground is long-term goal of this research [*Fishman et al.*, 2005] and clearly beyond the scope of the present study. However, we feel that this study has succeeded in showing that regional TOR distributions are influenced by prevailing meteorological conditions related to large-scale weather patterns and that this is the first step in attempting to forecast high tropospheric ozone levels on shorter timescales. In turn, using such information in a short-term predictive mode can mitigate the pollution's detrimental effects on human health.

[28] This study has used satellite data from two satellites originally designed in the 1970s that had not been intended to derive any information about tropospheric ozone. With the launch of the ESA's (European Space Agency) Envisat in 2002 and NASA's (National Aeronautics and Space Agency) Aura in 2004, new generations of instruments are measuring ozone and ozone pollution precursors with capabilities that provide much better resolution and accuracy. As the data from these satellites become available to the scientific community, we expect to glean even more insight into how regional and global pollution patterns evolve and how such patterns are related to prevailing meteorological conditions. Last, as these new measurements become available from these satellites, the data described in this study can also be used as a benchmark to quantify how atmospheric composition has been modified over decadal timescales.

[29] **Acknowledgment.** We appreciate comments on earlier versions of this paper from J. Ziemke, S. Chandra, and P. Bhartia, NASA Goddard Space Flight Center; M. Newchurch, University of Alabama-Huntsville; J. Lelieveld and M. Lawrence, Max-Planck-Institute for Chemistry; and V. Ramanathan, Scripps Institute of Oceanography.

References

Al-Saadi, J., et al. (2005), Improving national air quality forecasts with satellite aerosol observations, *Bull. Am. Meteorol. Soc.*, *86*, 1249–1261.

Bell, M. L., A. McDermott, S. L. Zeger, J. M. Samet, and F. Dominici (2004), Ozone and short-term mortality in 95 U.S. urban communities, *J. Am. Med. Assoc.*, *292*(19), 2372–2378.

Boersma, K. F., H. J. Eskes, and E. J. Brinksma (2004), Error analysis for tropospheric NO_2 retrieval from space, *J. Geophys. Res.*, *109*, D04311, doi:10.1029/2003JD003962.

Bowman, K. P. (1989), Global patterns of the quasi-biennial oscillation in total ozone, *J. Atmos. Sci.*, *46*, 3328–3343.

Chameides, W. L., et al. (1999), Is ozone pollution affecting crop yields in China, *Geophys. Res. Lett.*, *26*, 867–870.

Chandra, S., and R. S. Stolarski (1991), Recent trends in stratospheric total ozone: Implications of dynamical and El Chichon perturbations, *Geophys. Res. Lett.*, *18*, 227–2280.

Cheung, V. T. F., and T. Wang (2001), Observational study of ozone pollution at a rural site in the Yangtze Delta of China, *Atmos. Environ.*, *35*, 4947–4958.

Cook, K. H. (1999), Generation of the African easterly jet and its role in determining West African precipitation, *J. Clim.*, *12*, 1165–1184.

Creilson, J. K., J. Fishman, and A. E. Wozniak (2003), Intercontinental transport of tropospheric ozone: A study of its seasonal variability across the North Atlantic and its relationship to the North Atlantic Oscillation, *Atmos. Chem. Phys.*, *3*, 2053–2066.

Dabberdt, W. F., et al. (2004), Meteorological research needs for improved air quality forecasting: Report of the 11th Prospectus Development Team of the U.S. Weather Research Program, *Bull. Am. Meteorol. Soc.*, *85*, 563–586.

de Gouw, J. A., et al. (2001), Overview of the trace gas measurements on board the Citation aircraft during the intensive field phase of INDOEX, *J. Geophys. Res.*, *106*, 28,453–28,468.

Di Girolamo, L., et al. (2004), Analysis of Multi-angle Imaging Spectro-Radiometer (MISR) aerosol optical depths over greater India during winter 2001–2004, *Geophys. Res. Lett.*, *31*, L23115, doi:10.1029/2004GL021273.

Duncan, B. N., R. V. Martin, A. C. Staudt, R. Yevich, and J. A. Logan (2003), Interannual and seasonal variability of biomass burning emissions constrained by satellite observations, *J. Geophys. Res.*, *108*(D2), 4100, doi:10.1029/2002JD002378.

Edwards, D. P., et al. (2003), Tropospheric ozone over the tropical Atlantic: A satellite perspective, *J. Geophys. Res.*, *108*(D8), 4237, doi:10.1029/2002JD002927.

Fishman, J., and A. E. Balok (1999), Calculation of daily tropospheric ozone residuals using TOMS and empirically improved SBUV measurements, *J. Geophys. Res.*, *104*, 30,319–30,340.

Fishman, J., F. M. Vukovich, D. R. Cahoon, and M. C. Shipham (1987), The characterization of an air pollution episode using satellite total ozone measurements, *J. Clim. Appl. Meteorol.*, *26*, 1638–1654.

Fishman, J., A. E. Wozniak, and J. K. Creilson (2003), Global distribution of tropospheric ozone from satellite measurements using the empirically corrected tropospheric ozone residual technique: Identification of the regional aspects of air pollution, *Atmos. Chem. Phys.*, *3*, 893–907.

Fishman, J., D. P. McNamara, J. J. Szykman, A. E. Wozniak, and J. K. Creilson (2005), An exploratory study to use OMI total ozone data in near-real-time to produce a guidance product or air quality forecasters, paper presented at EOS Aura Science Team Meeting, Natl. Aeronaut. and Space Admin., Pasadena, Calif.

Frankenberg, C., U. Platt, and T. Wagner (2005), Retrieval of CO from SCIAMACHY onboard ENVISAT: Detection of strongly polluted areas and seasonal patterns in global CO abundances, *Atmos. Chem. Phys.*, *5*, 1639–1644.

Goswami, B. N., and R. S. A. Mohan (2001), Intraseasonal oscillations and interannual variability of the Indian summer monsoon, *J. Clim.*, *14*, 1180–1198.

Grist, J. P., and S. E. Nicholson (2001), A study of the dynamic factors influencing the rainfall variability in the west African Sahel, *J. Clim.*, *14*, 1337–1359.

Hasebe, F. (1996), Quasi-biennial oscillations of ozone and diabatic circulation in the equatorial stratosphere, *J. Atmos. Sci.*, *51*, 729–745.
Heck, W. H., R. M. Adams, W. W. Cure, A. S. Hoagle, H. E. Heggestad, R. Kohut, L. W. Kress, J. O. Rawlings, and O. C. Taylor (1983), A reassessment of crop loss from ozone, *Environ. Sci. Technol.*, *17*, 573A–581A.
Ju, J., and J. Slingo (1995), The Asian summer monsoon and ENSO, *Q. J. R. Meteorol. Soc.*, *121*, 1133–1168.
Kalnay, E., et al. (1996), The NCEP/NCAR Reanalysis 40-year Project, *Bull. Am. Meteorol. Soc.*, *77*, 437–471.
Kinnersley, J. S., and K.-K. Tung (1998), Modeling the global interannual variability of ozone due to the equatorial QBO and to extratropical planetary wave variability, *J. Atmos. Sci.*, *55*, 1417–1428.
Koren, H. S., et al. (1989), Ozone-induced inflammation in the lower airways of human subjects, *Am. Rev. Respir. Dis.*, *139*, 407–415.
Krishnamurthy, V., and J. Shukla (2000), Intraseasonal and interannual variability of rainfall over India, *J. Clim.*, *13*, 4366–4377.
Lelieveld, J., et al. (2001), The Indian Ocean experiment: Widespread air pollution from South and Southeast Asia, *Science*, *291*, 1031–1036.
Lindzen, R. S., and J. R. Holton (1968), A theory of the quasi-biennial oscillation, *J. Atmos. Sci.*, *25*, 1095–1107.
Lippmann, M., and R. B. Schlesinger (2000), Toxicological bases for the setting of health-related pollution standards, *Annu. Rev. Public Health*, *21*, 309–333.
Logan, J. A. (1999), An analysis of ozonesonde data for the troposphere: Recommendations for testing 3-D models, and development of a gridded climatology for tropospheric ozone, *J. Geophys. Res.*, *104*, 16,115–16,149.
Nicholson, S. E., and J. P. Grist (2003), The seasonal evolution of the atmospheric circulation over West Africa and equatorial Africa, *J. Clim.*, *16*, 1013–1030.
Nicholson, S. E., and J. Kim (1997), The relationship of the El Niño-Southern Oscillation to African rainfall, *Int. J. Climatol.*, *17*, 117–135.
Palmer, T. N., C. Brankovic, P. Viterbo, and M. J. Miller (1992), Modeling interannual variations of summer monsoons, *J. Clim.*, *5*, 399–417.
Parthasarathy, B., A. A. Munot, and D. R. Kothawale (1995), Monthly and seasonal rainfall series for all-India homogeneous regions and meteorological subdivisions: 1871–1994, *Res. Rep. RR-065*, Ind. Inst. of Trop. Meteorol., Pune, India.
Philander, S. G. H. (1990), *El Niño, La Niña, and the Southern Oscillation*, *Int. Geophys. Ser.*, vol. 46, 289 pp., Elsevier, New York.
Ramanathan, V., et al. (2001), Indian Ocean experiment: An integrated analysis of the climate forcing and effects of the great Indo-Asian haze, *J. Geophys. Res.*, *106*, 28,371–28,398.
Randel, W. J., and F. Wu (1996), Isolation of ozone QBO in SAGE II data by singular-value decomposition, *J. Atmos. Sci.*, *53*, 2546–2559.
Rasmusson, E. M., and T. H. Carpenter (1983), The relationship between eastern equatorial Pacific sea surface temperatures and rainfall over India and Sri Lanka, *Mon. Weather Rev.*, *111*, 517–528.
Reed, R. J. (1965), The quasi-biennial oscillation of the atmosphere between 30 and 50 km over Ascension Island, *J. Atmos. Sci.*, *22*, 331–333.
Shukla, J., and J. M. Wallace (1983), Numerical simulation of the atmospheric response to equatorial Pacific sea surface temperature anomalies, *J. Atmos. Sci.*, *40*, 1613–1630.
Skelly, J. M. (2000), Tropospheric ozone and its importance to forests and natural plant communities of the northeastern United States, *Northeast. Nat.*, *3*, 221–236.
Spektor, D. M., M. Lippmann, P. J. Lioy, G. D. Thurston, K. Citak, D. J. James, N. Bock, F. E. Speizer, and C. Hayes (1988), Effects of ambient ozone on respiratory function in active, normal children, *Am. Rev. Respir. Dis.*, *137*, 313–320.
Staehelin, J., J. Thudium, R. Buhler, A. Volz-Thomas, and W. Gräber (1994), Trends in surface ozone concentrations at Arosa (Switzerland), *Atmos. Environ.*, *28*, 75–87.
Szykman, J., J. White, R. Pierce, J. Al-Saadi, D. Neil, C. Kittaka, D. Chu, L. Remer, L. Gumley, and E. Prins (2004), Utilizing MODIS satellite observations in near-real-time to improve AIRNOW next day forecast of fine particulate matter, paper presented at Sixth Conference on Atmospheric Chemistry, Am. Meteorol. Soc., Seattle, Wash.
Torres, O., and P. K. Bhartia (1999), Impact of tropospheric aerosol absorption on ozone retrieval from backscattered ultraviolet measurements, *J. Geophys. Res.*, *104*, 21,569–21,577.
Tung, K.-K., and H. Yang (1994), Global QBO in circulation and ozone: Part I. Reexamination of observational evidence, *J. Atmos. Sci.*, *51*, 2699–2707.
van Aardenne, J. A., G. R. Carmichael, H. Levy II, D. Streets, and L. Hordijk (1999), Anthropogenic NO_x emissions in Asia in the period 1990–2020, *Atmos. Environ.*, *33*, 633–646.
Volz, A., and D. Kley (1988), Evaluation of the Montsouris series of ozone measurements made in the nineteenth century, *Nature*, *332*, 240–242.
Webster, P. J., and S. Yang (1992), Monsoon and ENSO: Selectively interactive systems, *Q. J. R. Meteorol. Soc.*, *118*, 877–926.
Wozniak, A. E., J. Fishman, P.-H. Wang, and J. K. Creilson (2005), Distribution of stratospheric column ozone (SCO) determined from satellite observations: Validation of solar backscatter ultraviolet (SBUV) measurements in support of the tropospheric ozone residual (TOR) method, *J. Geophys. Res.*, *110*, D20305, doi:10.1029/2005JD005842.
Ziemke, J. R., and S. Chandra (2003), La Niña and El Niño–induced variabilities of ozone in the tropical lower atmosphere during 1970–2001, *Geophys. Res. Lett.*, *30*(3), 1142, doi:10.1029/2002GL016387.

J. K. Creilson, J. Fishman, and A. E. Wozniak, NASA Langley Research Center, Mail Stop 401A, Hampton, VA 23681, USA. (j.k.creilson@larc.nasa.gov; jack.fishman@nasa.gov; a.e.wozniak@larc.nasa.gov)

P. J. Crutzen, Max-Planck-Institute for Chemistry, P.O. Box 3060, Mainz, Germany, D-55020. (air@mpch-mainz.mpg.de)